

Nonmagnetic Impurity Resonances as a Signature of Sign-Reversal Pairing in the FeAs-based Superconductors

Degang Zhang¹

¹*Texas Center for Superconductivity and Department of Physics,
University of Houston, Houston, TX 77204, USA*

The low energy band structure of the FeAs based superconductors is fitted by a tight binding model with two Fe ions per unit cell and two degenerate orbitals per Fe ion. Based on this, superconductivity with extended s-wave pairing symmetry of the form $\cos k_x + \cos k_y$ is examined. The local density of states near an impurity is also investigated by using T-matrix approach. For the nonmagnetic scattering potential, we found that there exist two major resonances inside the gap. The height of the resonance peaks depends on the strength of the impurity potential. These in-gap resonances are originated in the Andreev's bound states due to the quasiparticle scattering between the hole Fermi surfaces around Γ point with positive order parameter and the electron Fermi surfaces around M point with negative order parameter.

PACS numbers: 71.10.Fd, 71.18.+y, 71.20.-b, 74.20.-z

The recent discovery of a new family of superconductors, i.e. the FeAs based superconductors [1-6], has attracted much attention in the condensed matter community. It has been reported that the superconducting transition temperature T_c can be obtained as high as 55K [2]. The undoped iron arsenides have a spin density wave order below 150K [4]. When holes or electrons are doped, the iron arsenides become superconducting.

Similar to the cuprate superconductors, the FeAs based superconductors also have a layer structure. It has been accepted that superconductivity comes from the Cooper pairs in the Fe-Fe plane. However, in the FeAs based superconductors, each unit cell contains two Fe ions and two As ions. The four As ions around each Fe ion do not locate in the Fe-Fe plane and have a two-fold rotation symmetry and two reflection symmetries (see Fig. 1). Due to different arrays of As ions around Fe ions, the Fe-Fe plane can be divided into two sublattices A and B. We note that the diagonal directions of the Fe-Fe plane have the translational symmetry with the period a . In this coordinate system, the momentum is a good quantum number.

Angle resolved photoemission spectroscopy (ARPES) experiments have probed the electronic properties in the FeAs-based superconductors [7-15]. It is established that there are two hole Fermi surfaces around (0,0) and two electron Fermi surfaces around (π, π) . These Fermi surface characteristics have been obtained by the LDA calculations [16-19]. Many theoretical models have been presented to reproduce the hole and electron pockets by employing the Fe d and As p orbitals and the hybridization among them [20-25]. However, there is no consensus on the superconducting gaps on the Fermi surfaces. In a series of ARPES, scanning tunneling microscopy (STM) experiments, and point-contact Andreev reflection spectroscopy experiments, the order parameter has been interpreted to be nodeless [7,9-15,26], nodal [27-29], single gap [10,26,29-32], and multiply gaps [7,11-15].

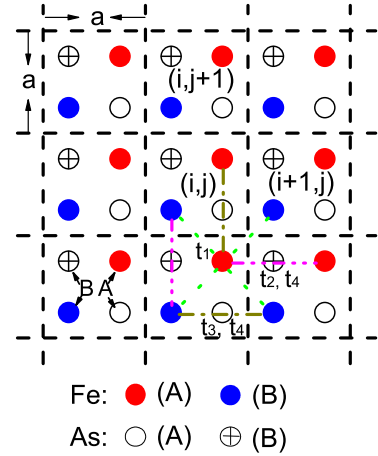


FIG. 1: (Color online) Schematic lattice structure of the FeAs layers with each unit cell (denoted by i and j) containing two Fe (A and B) and two As (A and B) ions. The As ions A and B are located just above and below the center of each face of the Fe square lattice, respectively. Here, t_1 is the nearest neighboring hopping between the same orbitals d_{xz} or d_{yz} . t_2 and t_3 are the next nearest neighboring hoppings between the same orbitals mediated by the As ions B and A, respectively. t_4 is the next nearest neighboring hopping between the different orbitals.

In this work, we start from two Fe ions per unit cell and two degenerate orbitals d_{xz} and d_{yz} per Fe ion and construct an effective four-band model, which exhibits the features of the Fermi surfaces in the FeAs-based superconductors. Based on the mean field theory for superconductivity, we investigate the differential conductance and the impurity effect for the extended s-wave pairing symmetry [12,17,20], so that we can understand the elec-

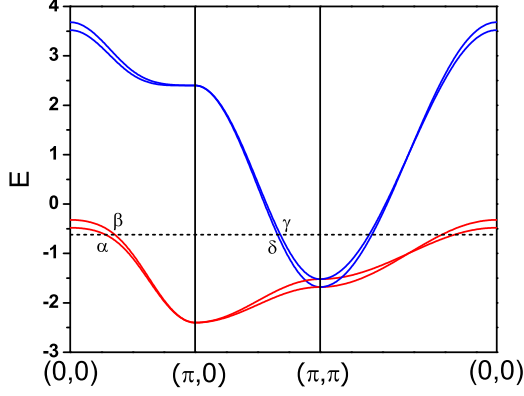


FIG. 2: (Color online) The band structure of the four-band model with $t_1 = 0.5, t_2 = 0.2, t_3 = -1.0, t_4 = 0.02$, and $\mu = -0.622$ (eV), plotted along the path $(0,0) \rightarrow (\pi,0) \rightarrow (\pi,\pi) \rightarrow (0,0)$.

tronic properties in the FeAs-based superconductors.

We assume that t_1 is the hopping between the same orbitals on the nearest neighboring Fe sites, t_2 and t_3 are the next nearest neighboring hoppings between the same orbitals mediated by As ions B and A, respectively, and t_4 is the hopping between the different orbitals on the next nearest neighboring Fe sites (see Fig. 1). It is expected that t_4 is small and has the same value in both translation symmetry directions. Therefore, the model Hamiltonian we propose can be written as

$$\begin{aligned}
 H_0 = & - \sum_{\alpha i j \sigma} \{ \mu (c_{A\alpha,ij\sigma}^+ c_{A\alpha,ij\sigma} + c_{B\alpha,ij\sigma}^+ c_{B\alpha,ij\sigma}) \\
 & + [t_1 c_{A\alpha,ij\sigma}^+ (c_{B\alpha,ij\sigma} + c_{B\alpha,i+1j\sigma} + c_{B\alpha,ij+1\sigma} + c_{B\alpha,i+1j+1\sigma}) \\
 & + t_2 (c_{A\alpha,ij\sigma}^+ c_{A\alpha,i+1j\sigma} + c_{B\alpha,ij\sigma}^+ c_{B\alpha,ij+1\sigma}) \\
 & + t_3 (c_{A\alpha,ij\sigma}^+ c_{A\alpha,ij+1\sigma} + c_{B\alpha,ij\sigma}^+ c_{B\alpha,i+1j\sigma}) \\
 & + t_4 (c_{A\alpha,ij\sigma}^+ c_{A\alpha+1,i+1j\sigma} + c_{A\alpha,ij\sigma}^+ c_{A\alpha+1,ij+1\sigma} \\
 & + c_{B\alpha,ij\sigma}^+ c_{B\alpha+1,i+1j\sigma} + c_{B\alpha,ij\sigma}^+ c_{B\alpha+1,ij+1\sigma}) + \text{h.c.}] \}, \quad (1)
 \end{aligned}$$

where σ is the spin index, i, j label the position of unit cell, and $\alpha = 0$ and 1 represent the degenerate orbitals d_{xz} and d_{yz} , respectively. Obviously, H_0 possesses the same symmetry with the FeAs-based superconductors, which is key to understand the electronic properties of this new family of high temperature superconductors.

By diagonalizing the above Hamiltonian in the momentum space, one obtains

$$\begin{aligned}
 H_0 = & \sum_{uv\mathbf{k}\sigma} (E_{uv,\mathbf{k}} - \mu) \psi_{uv,\mathbf{k}\sigma}^+ \psi_{uv,\mathbf{k}\sigma}, \\
 E_{uv,\mathbf{k}} = & \frac{1}{2} (\epsilon_{A,\mathbf{k}} + \epsilon_{B,\mathbf{k}}) + (-1)^v \epsilon_{xy,\mathbf{k}} \\
 & + (-1)^u \sqrt{\frac{1}{4} (\epsilon_{A,\mathbf{k}} - \epsilon_{B,\mathbf{k}})^2 + \epsilon_{T,\mathbf{k}} \epsilon_{T,\mathbf{k}}^*}, \quad (2)
 \end{aligned}$$

where $u(v) = 0, 1$, $\epsilon_{A,\mathbf{k}} = -2(t_2 \cos k_x + t_3 \cos k_y)$, $\epsilon_{B,\mathbf{k}} = -2(t_2 \cos k_y + t_3 \cos k_x)$, $\epsilon_{xy,\mathbf{k}} = -2t_4(\cos k_x + \cos k_y)$ and $\epsilon_{T,\mathbf{k}} = -t_1[1 + e^{ik_x} + e^{ik_y} + e^{i(k_x+k_y)}]$. Here, we have set the lattice constant $a = 1$. In deriving Eq. (2), we have introduced $c_{A(B)\alpha,ij\sigma} = \frac{1}{\sqrt{N}} \sum_{\mathbf{k}} c_{A(B)\alpha,\mathbf{k}\sigma} e^{i(k_x x_i + k_y y_j)}$ and have taken the canonical transformation

$$\begin{pmatrix} c_{A0,\mathbf{k}\sigma} \\ c_{A1,\mathbf{k}\sigma} \\ c_{B0,\mathbf{k}\sigma} \\ c_{B1,\mathbf{k}\sigma} \end{pmatrix} = \begin{pmatrix} \frac{a_{0,\mathbf{k}}}{\Gamma_{0,\mathbf{k}}} & \frac{a_{0,\mathbf{k}}}{\Gamma_{0,\mathbf{k}}} & \frac{a_{1,\mathbf{k}}}{\Gamma_{1,\mathbf{k}}} & \frac{a_{1,\mathbf{k}}}{\Gamma_{1,\mathbf{k}}} \\ \frac{a_{0,\mathbf{k}}}{\Gamma_{0,\mathbf{k}}} & -\frac{a_{0,\mathbf{k}}}{\Gamma_{0,\mathbf{k}}} & \frac{a_{1,\mathbf{k}}}{\Gamma_{1,\mathbf{k}}} & -\frac{a_{1,\mathbf{k}}}{\Gamma_{1,\mathbf{k}}} \\ \frac{\epsilon_{T,\mathbf{k}}^*}{\Gamma_{0,\mathbf{k}}} & \frac{\epsilon_{T,\mathbf{k}}^*}{\Gamma_{0,\mathbf{k}}} & \frac{\epsilon_{T,\mathbf{k}}^*}{\Gamma_{1,\mathbf{k}}} & \frac{\epsilon_{T,\mathbf{k}}^*}{\Gamma_{1,\mathbf{k}}} \\ \frac{\epsilon_{T,\mathbf{k}}^*}{\Gamma_{0,\mathbf{k}}} & -\frac{\epsilon_{T,\mathbf{k}}^*}{\Gamma_{0,\mathbf{k}}} & \frac{\epsilon_{T,\mathbf{k}}^*}{\Gamma_{1,\mathbf{k}}} & -\frac{\epsilon_{T,\mathbf{k}}^*}{\Gamma_{1,\mathbf{k}}} \end{pmatrix} \begin{pmatrix} \psi_{00,\mathbf{k}\sigma} \\ \psi_{01,\mathbf{k}\sigma} \\ \psi_{10,\mathbf{k}\sigma} \\ \psi_{11,\mathbf{k}\sigma} \end{pmatrix}, \quad (3)$$

where $\Gamma_{u,\mathbf{k}} = \sqrt{2(a_{u,\mathbf{k}}^2 + \epsilon_{T,\mathbf{k}} \epsilon_{T,\mathbf{k}}^*)}$ and $a_{u,\mathbf{k}} = \frac{1}{2}(\epsilon_{A,\mathbf{k}} - \epsilon_{B,\mathbf{k}}) + (-1)^u \sqrt{\frac{1}{4}(\epsilon_{A,\mathbf{k}} - \epsilon_{B,\mathbf{k}})^2 + \epsilon_{T,\mathbf{k}} \epsilon_{T,\mathbf{k}}^*}$.

Eq. (2) describes analytically four energy bands with the indexes u, v . In Fig. 2, we plot these bands along the path $(0,0) \rightarrow (\pi,0) \rightarrow (\pi,\pi) \rightarrow (0,0)$. In our calculations, we have used $t_1 = 0.5, t_2 = 0.2, t_3 = -1.0, t_4 = 0.02$, and $\mu = -0.622$ (half filling) (eV). Obviously, there exist two hole Fermi surfaces around $(0,0)$, i.e. α - and β -bands, and two electron Fermi surfaces around (π,π) , i.e. γ - and δ -bands. This is consistent with those observed from ARPES experiments [7-15]. We note that the hole and electron pockets are associated with $u = 1$ and 0 while $v = 0$ and 1 represent the inner and outer Fermi surfaces of the hole and electron pockets, respectively. The parameters t_1, t_2 and t_3 determine the sizes of the hole and electron pockets, and t_4 controls the intervals between the inner and outer Fermi surfaces. We note that $\mu < -0.622$ and $\mu > -0.622$ correspond to hole and electron dopings, respectively. When hole (electron) doping increases, the hole (electron) Fermi surfaces, i.e. α - and β -bands (γ - and δ -bands), become larger while the electron (hole) Fermi surfaces i.e. γ - and δ -bands (α - and β -bands) become smaller. The variation of the Fermi surfaces with hole or electron doping has been observed by ARPES experiments [7-15]. When $\mu > -0.32$ (i.e. $\sim 26.5\%$ electron doping), β -band disappears.

In order to investigate superconductivity in iron arsenides, we now introduce the mean field BCS Hamiltonian

$$H_{SC} = \sum_{uv\mathbf{k}} (\Delta_{uv,\mathbf{k}} \psi_{uv,\mathbf{k}\uparrow}^+ \psi_{uv,-\mathbf{k}\downarrow}^+ + \text{h.c.}), \quad (4)$$

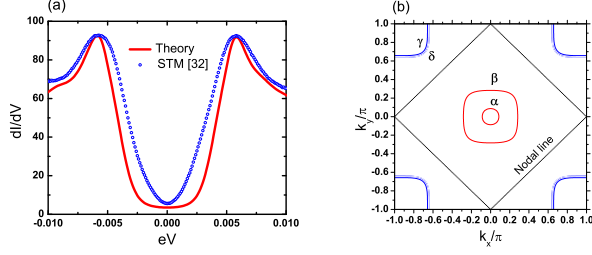


FIG. 3: (Color online) (a) The differential conductance as a function of the bias voltage eV for the pairing symmetry $\Delta_{uv,\mathbf{k}} = \frac{1}{2}\Delta_0(\cos k_x + \cos k_y)$ with $\Delta_0 = 5.8$ meV and $|\Delta_{uv,\mathbf{k}}|$ at optimal electron doping ($\sim 15\%$) under temperature 4.2K. (b) The corresponding Fermi surfaces.

where $\Delta_{uv,\mathbf{k}}$ are the superconducting gaps on the energy bands $<u, v>$, depending on the momentum of the long-lived quasiparticles $\psi_{uv,\mathbf{k}\sigma}$. We can see from Eqs. (3) and (4) that both inter- and intra-band pairings in the original electron operators $c_{A\alpha,\mathbf{k}\sigma}$ and $c_{B\alpha,\mathbf{k}\sigma}$ are automatically included. Here, we assume that the pairing potential between electrons is unique, which can avoid many superconducting transition temperatures [33]. In other words, the energy gaps on all the Fermi surfaces can be fitted by a single function of the momentum, i.e. $\Delta_{10,\mathbf{k}} = \Delta_{11,\mathbf{k}} = \Delta_{00,\mathbf{k}} = \Delta_{01,\mathbf{k}}$. In Ref. [12], Nakayama *et al.* measured the energy gaps on different Fermi surfaces in optimally hole-doped $\text{Ba}_{0.6}\text{K}_{0.4}\text{Fe}_2\text{As}_2$ ($T_c \sim 37\text{K}$) by employing ARPES experiments. The order parameter can be fitted as $\Delta_{uv,\mathbf{k}} = \frac{1}{2}\Delta_0(\cos k_x + \cos k_y)$ with $\Delta_0 = 13.5$ meV or $|\Delta_{uv,\mathbf{k}}|$. However, in the STM experiments on optimally electron-doped $\text{BaFe}_{1.8}\text{Co}_{0.2}\text{As}_2$ ($T_c \sim 22.5\text{K}$) [31,32], only two coherence peaks were observed at a small gap, i.e. $\sim \pm 5.8$ meV. In the following we shall calculate the differential conductance for the extended s-wave pairing symmetry in the optimal electron doping, so that we can compare our theory with the STM experiments.

After diagonalizing the Hamiltonian $H = H_0 + H_{SC}$ by the Bogoliubov transformation, we obtain the local density of states (LDOS) on the sublattices A or B

$$\rho_{A,B}(\omega) = -\frac{4}{N\pi} \sum_{uv\mathbf{k}\nu} \frac{\mathcal{A}_{u,\mathbf{k}}^{A,B} \xi_{uv,\mathbf{k}\nu}^2}{i\omega_n - (-1)^\nu \Omega_{uv,\mathbf{k}}} \Big|_{i\omega_n \rightarrow \omega + i0^+}, \quad (5)$$

where $\nu = \pm 1$, $\mathcal{A}_{u,\mathbf{k}}^A = a_{u,\mathbf{k}}^2/\Gamma_{u,\mathbf{k}}^2$, $\mathcal{A}_{u,\mathbf{k}}^B = \epsilon_{T,\mathbf{k}}\epsilon_{T,\mathbf{k}}^*/\Gamma_{u,\mathbf{k}}^2$, $\Omega_{uv,\mathbf{k}} = \sqrt{(E_{uv,\mathbf{k}} - \mu)^2 + \Delta_{uv,\mathbf{k}}^2}$, and $\xi_{uv,\mathbf{k}\nu}^2 = \frac{1}{2}[1 + (-1)^\nu \frac{E_{uv,\mathbf{k}} - \mu}{\Omega_{uv,\mathbf{k}}}]$. Obviously, the quasiparticles on the hole and electron pockets have different weights $\mathcal{A}_{u,\mathbf{k}}^{A,B}$ to contribute to the LDOS.

Usually the STM experiments are performed at low temperatures. In order to compare accurately with the STM experiments, we must take the effect of temperature

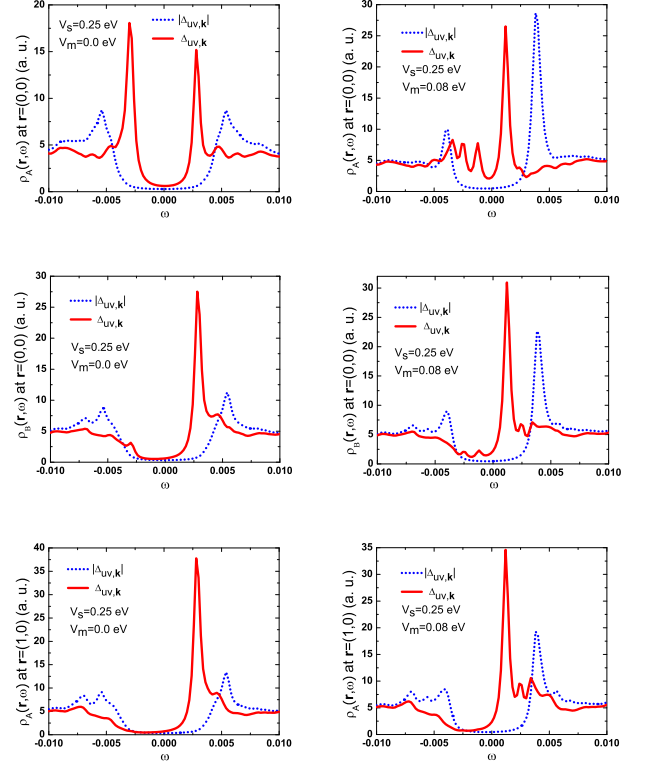


FIG. 4: (Color online) The LDOS near an impurity, which includes a dominant nonmagnetic potential V_s and a small magnetic part V_m , for the pairing symmetry $\Delta_{uv,\mathbf{k}} = \frac{1}{2}\Delta_0(\cos k_x + \cos k_y)$ with $\Delta_0 = 5.8$ meV and $|\Delta_{uv,\mathbf{k}}|$ at optimal electron doping ($\sim 15\%$).

into account. The differential conductance measured by the STM experiments is

$$\frac{dI}{dV} \propto - \int_{-\infty}^{\infty} f'(\omega - eV) \rho_{A,B}(\omega) d\omega, \quad (6)$$

where f' is the derivative of the Fermi function and V is the bias voltage applied between the STM tip and the sample.

According to the formulas (5) and (6), we can calculate the differential conductance with different pairing symmetries and dopings at low temperatures. In Fig. 3(a), we present the differential conductance for the extended s-wave symmetry with optimal electron doping under temperature 4.2K. We have observed that the main contribution to dI/dV comes from the hole Fermi surfaces, i.e. α - and β -bands. Therefore, whether or not the nodal points on γ - and δ -bands exist does not change qualitatively the features of dI/dV . The main difference between the theoretical results and the STM data could be due to the fact that either β - or δ - band of the STM sample is much closer to the nodal line as depicted in Fig. 3(b).

In order to detect the sign reversal pairing in the

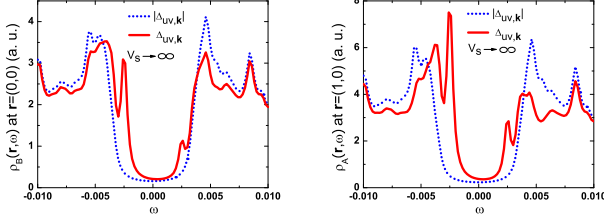


FIG. 5: (Color online) The LDOS near a unitary impurity for the pairing symmetry $\Delta_{uv,\mathbf{k}} = \frac{1}{2}\Delta_0(\cos k_x + \cos k_y)$ with $\Delta_0 = 5.8$ meV and $|\Delta_{uv,\mathbf{k}}|$ at optimal electron doping ($\sim 15\%$).

FeAs-based superconductors, now we calculate the LDOS near an impurity located at the origin of the sublattice A described by $H_{imp} = V_s \sum_{\alpha\sigma} c_{A\alpha,00\sigma}^\dagger c_{A\alpha,00\sigma} + V_m \sum_{\alpha} (c_{A\alpha,00\uparrow}^\dagger c_{A\alpha,00\uparrow} - c_{A\alpha,00\downarrow}^\dagger c_{A\alpha,00\downarrow})$. Here, V_s and V_m represent the nonmagnetic part and magnetic part of the impurity potential, respectively. The total Hamiltonian $H = H_0 + H_{SC} + H_{imp}$ can be solved by T-matrix approach [34]. The analytical expression for the LDOS on the sublattices A and B near the impurity has been derived and will be presented elsewhere [35]. We note that the inter-band scattering is only allowed for those bands with the same index v .

In Fig. 4, we plot the LDOS curves for $\Delta_{uv,\mathbf{k}}$ and $|\Delta_{uv,\mathbf{k}}|$ on and near the impurity site with a moderate strength of nonmagnetic potential, i.e. $V_s = 0.25$ eV, plus a small magnetic potential, i.e. $V_m = 0.08$ eV. Obviously, for a pure scattering potential ($V_m = 0$), the LDOS for $\Delta_{uv,\mathbf{k}}$ has two impurity resonance peaks at $\pm\omega_0 = \pm 2.8$ meV on the impurity site and has a sharp resonance peak at ω_0 near the impurity site. However, the LDOS for $|\Delta_{uv,\mathbf{k}}|$ has no such in-gap impurity states. Therefore, these impurity resonances can be used to detect the sign-reversal pairing in the FeAs-based superconductors. The origin of these impurity resonances comes from the Andreev's bound states due to the inter-band quasiparticle scattering with the phase opposite order parameters, similar to that of the zero bias resonance peak on the Zn impurity in cuprate superconductors. An additional small magnetic potential can strongly suppress the impurity peak at $-\omega_0$ and enhance the impurity peak at ω_0 on the impurity site. Meanwhile, all the resonance peaks on different sites slowly move forward to zero energy. We note that for the mixing potential, the LDOS for $|\Delta_{uv,\mathbf{k}}|$ is similar to that induced by a magnetic impurity in s-wave superconductors.

Fig. 5 shows the LDOS for $\Delta_{uv,\mathbf{k}}$ and $|\Delta_{uv,\mathbf{k}}|$ near the impurity site with a unitary potential. The LDOS for $\Delta_{uv,\mathbf{k}}$ also has two impurity resonance peaks at $\pm\omega_0$. However, the resonance peak at $-\omega_0$ is much stronger than that at ω_0 . For $|\Delta_{uv,\mathbf{k}}|$, the LDOS also has no in-gap impurity resonance peaks.

We also investigate the other cases of the impurity potential. For the attractive scattering potential, i.e. $V_s < 0$, the stronger resonance peak inside gap in the LDOS near the impurity site always appears at negative energy. With increasing $|V_s|$, the resonance peaks become higher. When $V_s \rightarrow -\infty$, the LDOS is identical with that for $V_s \rightarrow +\infty$, shown in Fig. 5. We note that an extra small magnetic potential does not change the features of the LDOS. For a dominantly magnetic potential, the LDOS near the impurity site for $\Delta_{uv,\mathbf{k}}$ has similar structures with that for $|\Delta_{uv,\mathbf{k}}|$, although the values of V_m or the locations of in-gap resonance peaks are different. Therefore, the magnetic impurity seems not to be good tool to detect the sign reversal pairing in the FeAs-based superconductors.

In summary, we have built a two-orbital four-band tight-binding model describing correctly the characteristics of the Fermi surfaces in the FeAs-based superconductors. In the framework of mean field theory, we have studied the differential conductance and the impurity effect for extended s-wave pairing symmetry. It is shown that the in-gap impurity resonances induced by nonmagnetic scattering potential can be regarded as a signature of sign-reversal pairing symmetry in the FeAs-based superconductors, which could be detected by STM experiments. These resonance peaks also exhibit in the overdoped and underdoped FeAs-based superconductors.

The author would like to thank C. S. Ting, S. H. Pan, Ang Li, and Tao Zhou for useful discussions, and especially S. H. Pan and Ang Li for providing me their STM data. This work was supported by the Texas Center for Superconductivity at the University of Houston and by the Robert A. Welch Foundation under the Grant no. E-1411.

-
- [1] Y. Kamihara *et al.*, J. Am. Chem. Soc. **130**, 3296 (2008).
 - [2] Z. A. Ren *et al.*, Chin. Phys. Lett. **25**, 2215 (2008).
 - [3] X. H. Chen *et al.*, Nature (London) **453**, 761 (2008).
 - [4] C. de la Cruz *et al.*, Nature (London) **453**, 899 (2008).
 - [5] G. F. Chen *et al.*, Phys. Rev. Lett. **100**, 247002 (2008).
 - [6] H.-H. Wen *et al.*, Europhys. Lett. **82**, 17009 (2008).
 - [7] H. Ding *et al.*, Europhys. Lett. **83**, 4701 (2008).
 - [8] D. H. Lu *et al.*, Nature (London) **455**, 81 (2008).
 - [9] C. Liu *et al.*, Phys. Rev. Lett. **101**, 177005 (2008).
 - [10] T. Kondo *et al.*, arXiv:0807.0815.
 - [11] D. V. Evtushinsky *et al.*, arXiv:0809.4455.
 - [12] K. Nakayama *et al.*, arXiv:0812.0663.
 - [13] V. B. Zabolotnyy *et al.*, Nature (London) **457**, 569 (2009).
 - [14] K. Terashima *et al.*, arXiv:0812.3704.
 - [15] Y. Sekiba *et al.*, arXiv:0812.4111.
 - [16] D. J. Singh and M. H. Du, Phys. Rev. Lett. **100**, 237003 (2008).
 - [17] I. I. Mazin *et al.*, Phys. Rev. Lett. **101**, 057003 (2008).
 - [18] K. Haule, J. H. Shim, and G. Kotliar, arXiv:0803.1279.
 - [19] G. Xu *et al.*, Europhys. Lett. **82**, 67002 (2008).

- [20] K. Kuroki *et al.*, Phys. Rev. Lett. **101**, 087004 (2008).
- [21] X. Dai, Z. Fang, Y. Zhou, and F.-C. Zhang, arXiv:0803.3982.
- [22] S. Raghu *et al.*, Phys. Rev. B **77**, 220503 (2008).
- [23] P. A. Lee and X.-G. Wen, arXiv:0804.1739.
- [24] Zi-Jian Yao, Jian-Xin Li, and Z. D. Wang, New J. Phys. **11**, 025009 (2009).
- [25] Y. Ran *et al.*, arXiv:0805.3535.
- [26] T.Y. Chen, Z. Teasnovic, R.H. Liu, X.H. Chen, and C.L. Chien, Nature (London) **453**, 1224 (2008).
- [27] L. Shan *et al.*, Europhys. Lett. **83**, 57004 (2008).
- [28] O. Millo *et al.*, Phys. Rev. B **78**, 092505 (2008).
- [29] M. C. Boyer *et al.*, arXiv:0806.4400.
- [30] M. H. Pan *et al.*, arXiv:0808.08950.
- [31] Y. Yin *et al.*, Phys. Rev. Lett. **102**, 097002 (2009).
- [32] S. H. Pan *et al.*, in preparation.
- [33] H. Suhl, B. T. Matthias, and L. R. Walker, Phys. Rev. Lett. **3**, 552 (1959).
- [34] A. V. Balatsky, I. Vekhter, and J.-X. Zhu, Rev. Mod. Phys. **78**, 373 (2006).
- [35] Degang Zhang, to be published.